Supporting Information

Multidimensional super-resolution microscopy unveils nanoscale surface aggregates in the aging of FUS condensates

Changdong He, Chun Ying Wu, Wan Li, Ke Xu*

Department of Chemistry, University of California, Berkeley, California 94720, United States.

* Correspondence to: xuk@berkeley.edu

Materials and Methods

Plasmid constructs

FUS was PCR-amplified from pDEST8_FLAGHA_FUS_HIS (Addgene plasmid no. 26375; a gift from Thomas Tuschl)[1]. The baculovirus transfer vector pFastBac HT was PCR-amplified from pFastBac HT JS-Munc18b (Addgene plasmid no. 135554; a gift from Jingshi Shen)[2]. pFastBac HT 10xHis-MBP-TEV-FUS was constructed by the Gibson assembly (New England BioLabs E2611) of pFastBac HT, PCR-amplified 10xHis-MBP (a gift from Eunyong Park), and PCR-amplified FUS. The FUS(G156E) mutation was generated by changing the glycine codon (GGA) to a glutamic acid codon (GAA) using PCR between the BamHI and XbaI sites. All constructed plasmids were prepared from XL1-Blue cells using the QIAprep Spin Miniprep Kit (QIAGEN). Protein-coding sequences were verified by Sanger sequencing at UC-Berkeley DNA Sequencing Facility. Baculoviruses carrying the above constructs were generated using the Bac-to-Bac Baculovirus Expression System (Thermo Fisher) following the provider's instructions.

Protein expression

The above 10xHis-MBP-TEV-FUS and 10xHis-MBP-TEV-FUS(G156E) baculovirus constructs were expressed in 500 mL Sf9 insect cells. After 96 hr, pellet was collected by spinning the cells at 2,000 rpm for 5 min. From here, all the purification steps were done at 4 ˚C until the protease cleavage step. The pellet was resuspended into 40 mL lysis buffer containing 50 mM Tris-HCl pH 7.4, 1 M KCl, 5% glycerol, and 10 mM imidazole. Protease inhibitors were added (Halt Protease Inhibitor Cocktail, Thermo Scientific 78429, excluding EDTA). The resuspended cells were lysed by sonication and clarified by centrifugation at 13,000 rpm for 30 min. The supernatant was collected and filtered with Corning syringe filters with a diameter of 28 mm and a pore size of 0.45 μm. The filtered supernatant was loaded onto 2 gravity columns each with 4 mL Ni-NTA agarose (Qiagen). The resin was pre-equilibrated with the lysis buffer. The protein was eluted with a buffer containing 50 mM Tris-HCl pH 7.4, 1 M KCl, 5% glycerol, and 250 mM imidazole. TEV protease (Sigma T4455) was added to the elute at a 1:50 ratio. The mixture was incubated at RT for 6 hr and then purified *via* gel filtration chromatography (ÄKTA go with Superdex-200 Increase 10/300 column, Cytiva) with the storage buffer containing 50 mM Tris-HCl pH 7.4, 500 mM KCl, 1 mM DTT and 5% glycerol. The peak fractions containing pure protein were concentrated by Amicon Ultra centrifugal filters (0.5 mL; 10 kDa MWCO) to ~1 mg/mL, aliquoted into PCR tubes, flash-frozen by liquid nitrogen, and stored at −80 ˚C.

Glass surface preparation for microscopy

The protocol was adapted from Gidi *et al*[3] and Nakashima *et al*[4]. #1.5 coverslips 12 mm in diameter and 24 × 50 mm in size were treated with a heated 3:1 H_2SO_4 (98%) and H_2O_2 (30%) mixture for 25 minutes, rinsed until neutral using Milli-Q water. The cleaned coverslips were sonicated in 0.5 M NaOH for 30 min, and rinsed until neutral using Milli-Q water. The coverslips were then sonicated in HPLC-grade acetone for 5 min, dried with N_2, and then placed in a covered Petri dish in an oven at 60 °C. Methoxy-PEG silane (MW 5000, PG1-SL-5k, Nanocs) was dissolved in dry DMSO at 30 mg mL^{-1} at 60 °C. The solution was added to the top side of the coverslips and incubated at 60 ˚C for 2 hr. Then, the coverslips were washed thoroughly with ethanol, MilliQ water (with 5 min sonication), and ethanol, dried with N_2, and then kept in the oven.

Preparation of condensate samples

An aliquot of the above FUS or FUS(G156E) stocks was thawed and spun at 13,000 rpm for 5 min. The supernatant was mixed at a 3:2 ratio with a crowding buffer [20% dextran (from *Leuconostoc* spp., Mr 450,000-

650,000; Sigma 31392) and 1 mM DTT in 50 mM Tris-HCl pH 7.4]. Single or combined dyes were pre-dissolved in the crowding buffer, including 1 μM of Nile Red (415711000, Acros Organics), 10 μM of CRANAD-2 (4803, Tocris), and 5 nM of Cy3B hydrolyzed from Cy3B-NHS ester (PA63101, Cytiva). The final mixture thus contained ~0.6 mg/mL FUS or FUS(G156E), 8% dextran, 300 mM KCl, 1 mM DTT, 3% glycerol in 50 mM Tris-HCl pH 7.4, and desired dyes. The sample was mixed thoroughly at room temperature on a bench rotor for 2 hr, and then sealed between two functionalized coverslips as described above. The resultant condensates were allowed to settle on the bottom coverslip, and the sample was kept in the dark at room temperature without further agitations. Brightfield and fluorescence microscopy showed no substantial changes in the condensate size over the aging process.

Optical setup

SMLM, SR-SMLM, and SM*d*M were performed on a home-built setup based on a Nikon Ti-E inverted fluorescence microscope, as described previously.[5,6] Briefly, a 642-nm laser (Stradus 642, Vortran, 110 mW) and two 561-nm lasers (OBIS 561 LS, Coherent, 150 mW and 200 mW) were coupled to the back focal plane of an oil-immersion objective lens (Nikon CFI Plan Apochromat lambda 100x, NA 1.45). A translational stage shifted the laser to the objective edge to enter the sample slightly below the critical angle of total internal reflection, an approach commonly known as pseudoTIRF or HILO.[7,8] The sample was thus illuminated and imaged in the wide field ~3 μm above the coverslip surface for a cross-section of the condensates.

SR-SMLM with Nile Red

For SR-SMLM with Nile Red[5], the sample was excited with the 561-nm laser at ~3 kW/cm^2. Wide-field emission was filtered with a long-pass filter (ET575lp, Chroma) and a short-pass filter (FF01-758/SP, Semrock), and cropped at the image plane to ~4 mm in width. The cropped intermediate image was collimated by an achromatic lens before being split into two paths with a 50:50 beam splitter (BSW10, Thorlabs). One of the two split paths was passed through an equilateral prism (PS863, Thorlabs) for spectral dispersion, and both paths were imaged onto two different halves of an EM-CCD camera (iXon Ultra 897, Andor) that recorded continuously in the frame-transfer mode at 110 frames per second (fps). The stochastic encountering of individual Nile Red molecules with hydrophobic phases in the sample led to bursts of single-molecule fluorescence emission, for which the above system concurrently recorded the images and spectra of the same molecules in the wide field. ~10^5 frames were recorded in ~15 min, and the accumulated single-molecule images and spectra were processed into SR-SMLM images, in which color was used to present the mean wavelength of local single-molecule spectra[5,9].

SM*d*M with Cy3B

For SM*d*M with Cy3B[6,10], a multifunction I/O board (PCI-6733, National Instruments) read the exposure timing of the EM-CCD camera, which recorded continuously at 110 fps, and accordingly modulated the 561-nm lasers to output tandem pulses across odd and even frames (Fig. 3a and Fig. S4ab). Typical center-to-center separation between the paired pulses was Δt = 4 ms, whereas the duration of each pulse was τ = 500 μs. The estimated peak and average power densities at the sample were ~15 and ~0.8 kW/cm^2, respectively. Wide-field fluorescence emission was filtered by a long-pass filter (ET575lp, Chroma) and a band-pass filter (ET605/70m, Chroma). Single-molecule images due to Cy3B molecules stochastically diffusing into the focal plane were thus captured during the pulse illumination time τ, and their displacements were evaluated over the fixed time interval Δt between the paired pulses. The above tandem excitation and recording scheme was repeated ~2×10^4 times in ~7 min, and the accumulated single-molecule displacements were spatially binned with a 120×120 nm^2 grid. To generate super-resolved maps of the local diffusion coefficient D, the distribution of displacements in each spatial

bin was separately fitted through maximum likelihood estimation (MLE) to a modified random-walk model with the probability distribution

$$P(r) = \frac{2r}{a}\exp(-\frac{r^2}{a}) + br \quad \text{(eqn. 1)}$$

where r is the single-molecule displacement, $a = 4D\Delta t$, and b is a background term to account for irrelevant molecules that randomly diffuse into the view, as rationalized and validated previously.[6] This model assumes a spatially uniform probability for background molecules to diffuse into the focal plane during Δt, and so the probability of finding a background molecule between r and $r + dr$ is proportional to $2\pi r dr$, which increases linearly with r.[6] However, for regions at the condensate surface, a substantial difference exists between the single-molecule densities inside and outside the condensates, and so the background term is less well fitted (*e.g.*, Fig. 3f). The fitted D values were color plotted on a continuous scale to generate spatial maps. To quantify the apparent two-component single-molecule displacements of Cy3B in the FUS-condensate interior, in this study we further introduce a new fitting model with the probability distribution

$$P(r) = F_1\frac{2r}{a_1}\exp(-\frac{r^2}{a_1}) + (1-F_1)\frac{2r}{a_2}\exp(-\frac{r^2}{a_2}) + br \quad \text{(eqn. 2)}$$

where F_1 and $F_2 = (1 - F_1)$ are the fractions of the two diffusivity components, and $a_1 = 4D_1\Delta t$ and $a_2 = 4D_2\Delta t$ account for the two diffusion coefficients D_1 and D_2. For presentation in Fig. 3hi, the fitted background term b was divided per F_1 and F_2 to be separately absorbed by the two diffusivity components for plotting.

SMLM with CRANAD-2

For SMLM of CRANAD-2, the sample was continuously illuminated with the 642-nm laser at ~4 kW/cm^2. Wide-field emission was filtered by a long-pass filter (ET655lp, Chroma) and a band-pass filter (ET705/100m, Chroma), and recorded with the EM-CCD camera at 110 fps. Bursts of single-molecule fluorescence emission were achieved as CRANAD-2 molecules stochastically bound and unbound from amyloid fibrils[11]. The camera recorded ~80,000 frames for each sample in ~12 min, and the localized single-molecule positions were assembled into SMLM images as described in [12,13]. For two-color imaging, the sample was first imaged for CRANAD-2 with the 642-nm excitation with the above emission filters. The filters were then switched to the above respective sets for Nile Red SMLM or Cy3B SM*d*M under 561-nm excitation.

Quantification of surface domains

CRANAD-2 and Nile Red SMLM images were imported into ImageJ, so that the centers and radii of the condensate droplets were identified by a plugin based on Hough transform.[14] These values were used to extract line profiles of single-molecule localization counts along the condensate circumferences as a function of the azimuth angle, *e.g.*, Fig. 2e. These profiles enabled the determination of segments with elevated molecular counts as surface aggregates. The surface coverage was then calculated for each droplet by dividing the total angles of aggregate occupancy by 360 degrees.

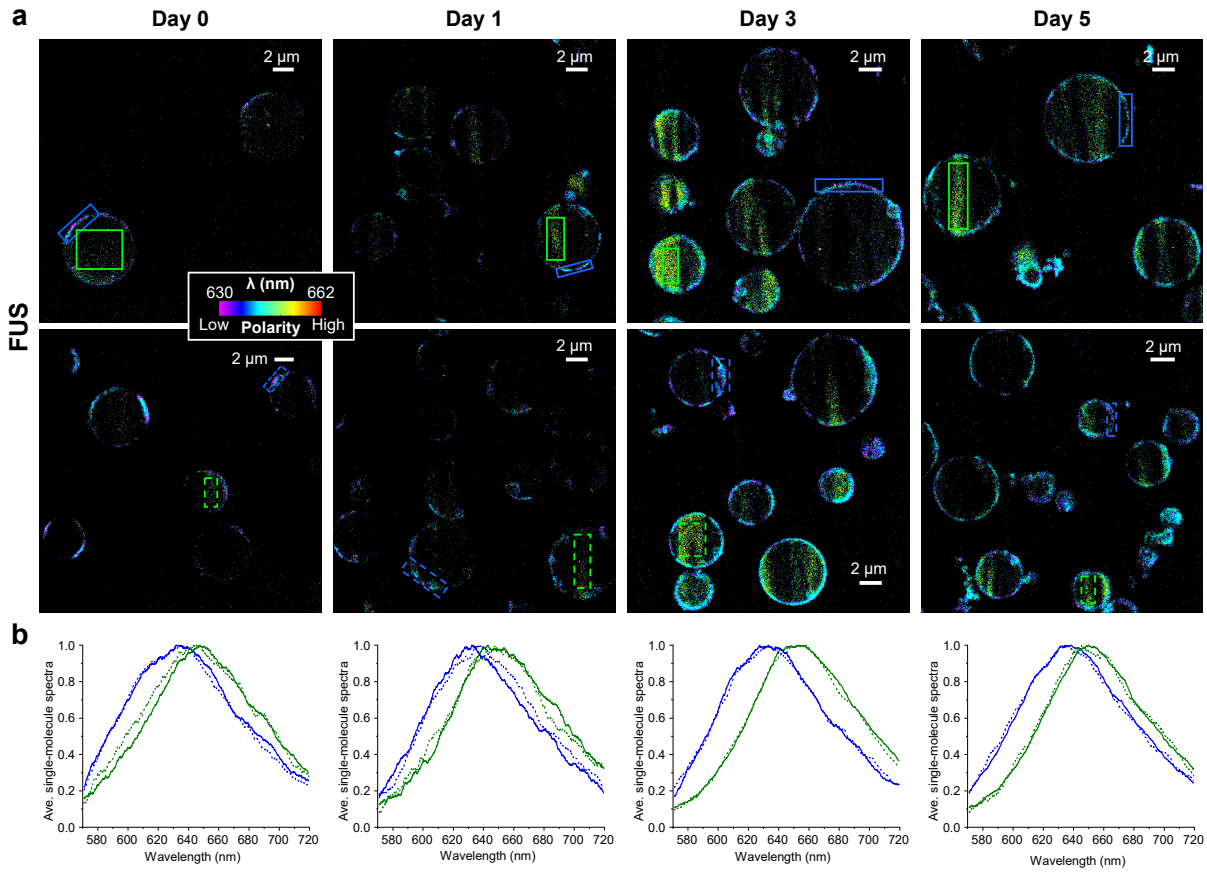

Fig. S1. Additional Nile Red SR-SMLM data for condensates of wild-type FUS. **a**. Color-coded Nile Red SR-SMLM images of FUS condensates aged for different days. Two representative images are shown for each timepoint in addition to the images shown in Fig. 1b. Color presents the mean wavelength of local single-molecule spectra (color scale bar), which reflects the local chemical polarity. **b**. Averaged single-molecule spectra at the condensate surface hydrophobic domains (blue) and the condensate interior (green) at different timepoints, for the sold-line and dash-line boxed regions in (a).

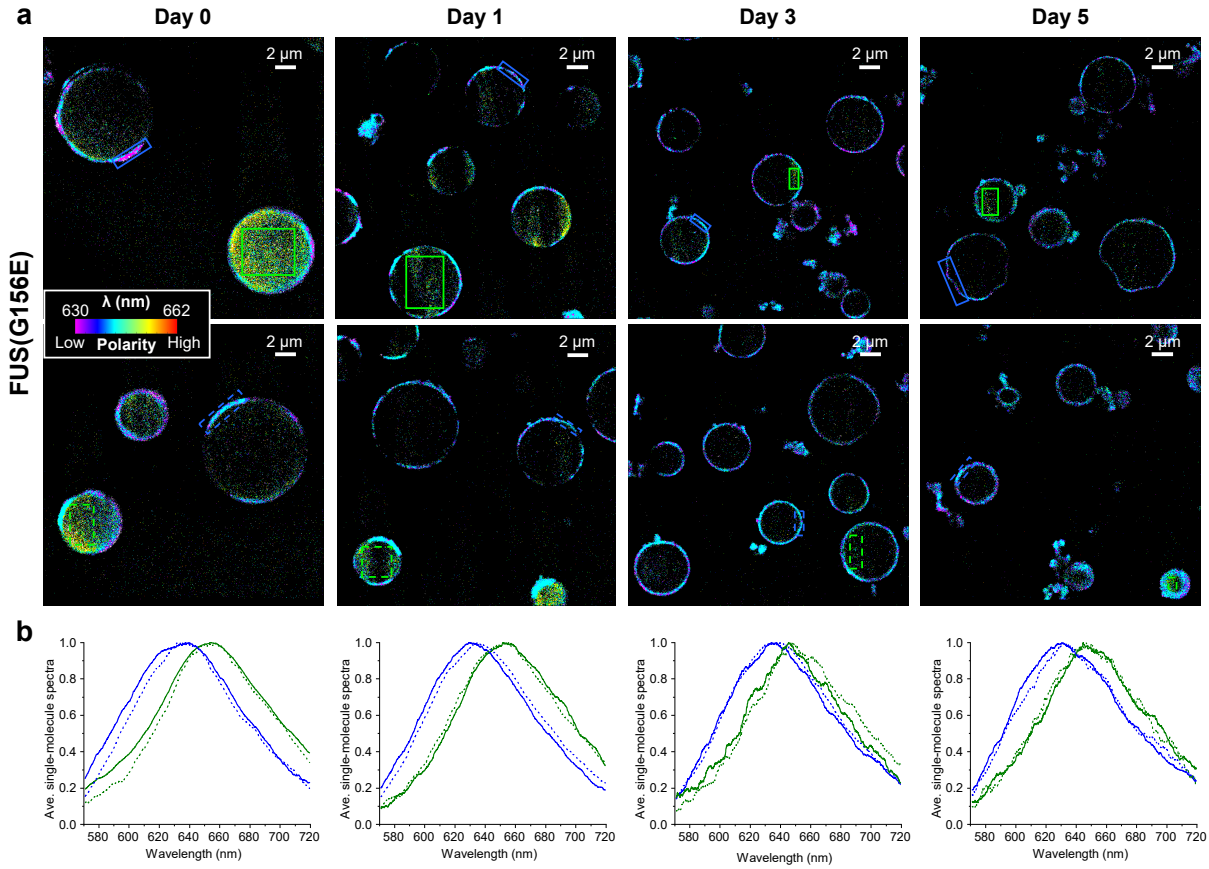

Fig. S2. Additional Nile Red SR-SMLM data for FUS(G156E) condensates. Figure is arranged the same way as Fig. S1.

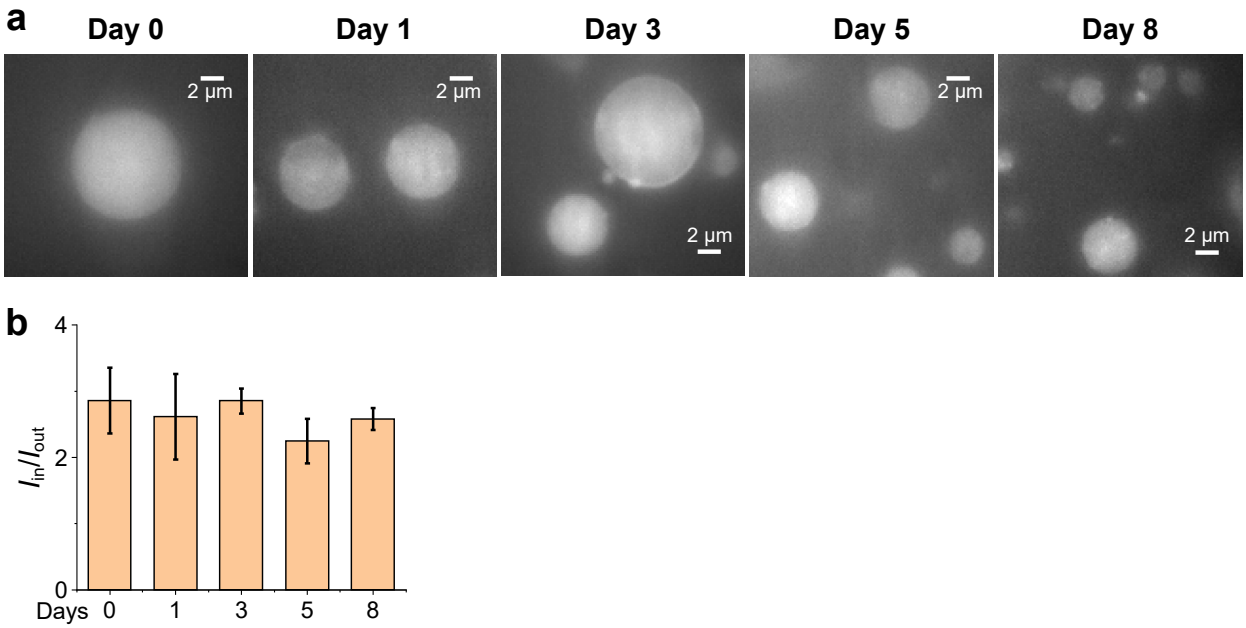

Fig. S3. Epifluorescence images of FUS condensate samples loaded with Cy3B. **a**. Epifluorescence images for samples aged for different days, corresponding to the same regions of SM*d*M data in Fig. 3d. **b**. Ratios of the detected intensities inside versus outside the condensates for samples aged for different days. Error bars: standard deviations between individual condensates. These results indicate that over the aging process, Cy3B maintains a fixed ~3-fold higher concentration in the condensates versus the outside dilute phase.

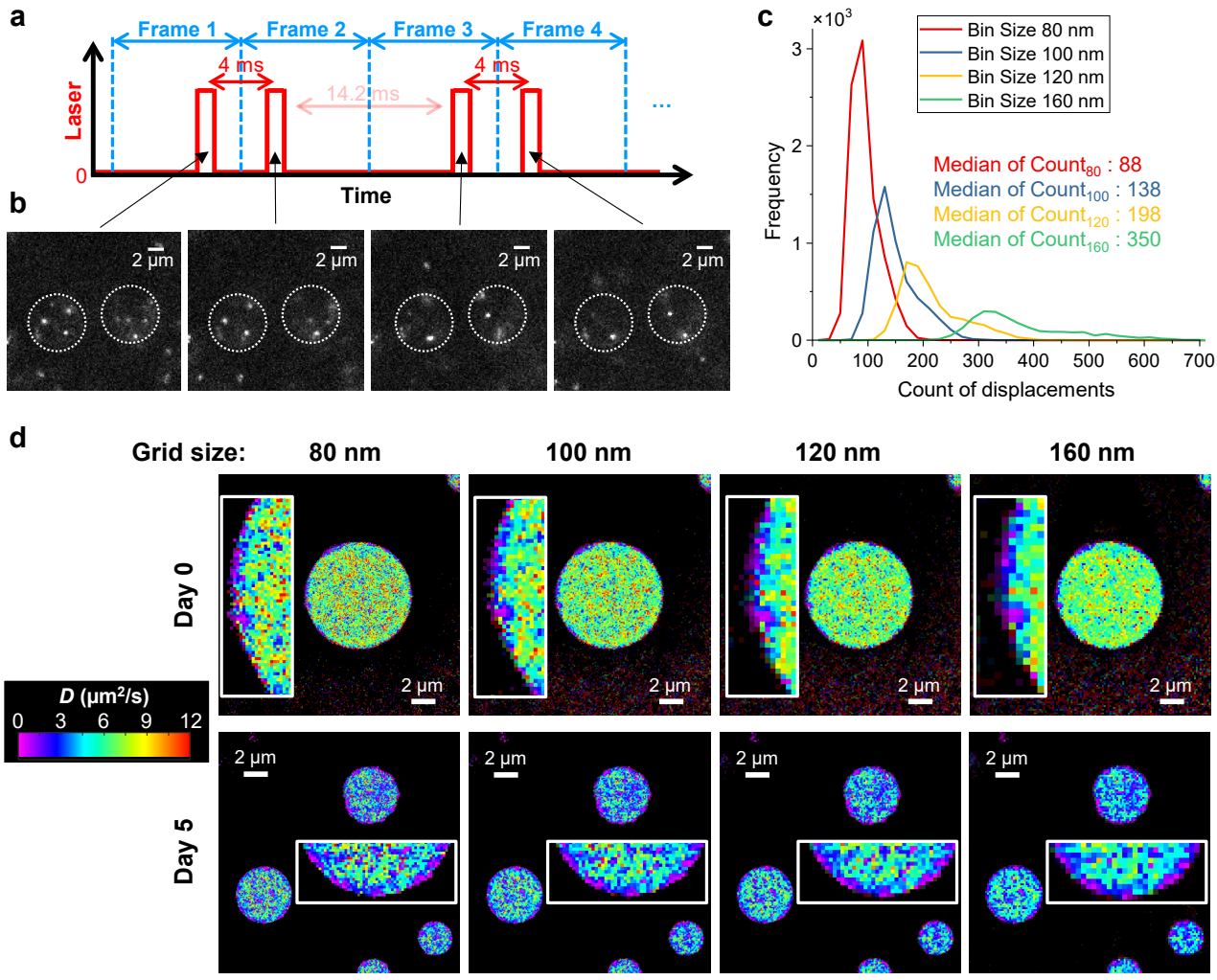

Fig. S4. Additional description and analysis of SM*d*M experiments. **a**. Typical illumination sequence used in this study for SM*d*M of Cy3B in FUS condensates, shown for two pairs of tandem frames. **b**. Example single-molecule images collected in such four consecutive frames. Dot lines outline the condensate droplets. The Δt = 4 ms center-to-center excitation separation between the paired frames (*e.g.*, Frames 1-2 and 3-4) allowed single-molecule displacements to be determined over Δt rather than the camera framerate. Meanwhile, the longer separations between the anti-paired frames (*e.g.*, Frames 2-3) allowed different molecules to diffuse into the focal plane to be sampled. **c**. Distributions of count of single-molecule displacements in each spatial bin at different grid sizes for the Day 0 condensate droplet shown in (d). **d**. SM*d*M diffusivity maps for Cy3B in FUS condensates on Day 0 and Day 5, analyzed with varied grid sizes of 80, 100, 120, and 160 nm. The 120 nm results duplicate that shown in Fig. 3d. These analyses indicate that low-diffusivity surface domains, as well as their growth in aging, are robustly observed for data processed with different grid sizes. Smaller grid sizes afford higher spatial resolutions at the expense of a reduced count of single-molecule displacements in each spatial bin and thus noisier *D* values.

Reference for supplement

(1) Hoell, J. I.; Larsson, E.; Runge, S.; Nusbaum, J. D.; Duggimpudi, S.; Farazi, T. A.; Hafner, M.; Borkhardt, A.; Sander, C.; Tuschl, T. RNA targets of wild-type and mutant FET family proteins. *Nat. Struct. Mol. Biol.* **2011**, *18*, 1428-1431.

(2) Yu, H.; Crisman, L.; Stowell, M. H. B.; Shen, J. Functional Reconstitution of Intracellular Vesicle Fusion Using Purified SNAREs and Sec1/Munc18 (SM) Proteins. *Methods Mol. Biol.* **2019**, *1860*, 237-249.

(3) Gidi, Y.; Bayram, S.; Ablenas, C. J.; Blum, A. S.; Cosa, G. Efficient One-Step PEG-Silane Passivation of Glass Surfaces for Single-Molecule Fluorescence Studies. *ACS Appl. Mater. Interfaces* **2018**, *10*, 39505-39511.

(4) Nakashima, K. K.; van Haren, M. H. I.; Andre, A. A. M.; Robu, I.; Spruijt, E. Active coacervate droplets are protocells that grow and resist Ostwald ripening. *Nat. Commun.* **2021**, *12*, 3819.

(5) Moon, S.; Yan, R.; Kenny, S. J.; Shyu, Y.; Xiang, L.; Li, W.; Xu, K. Spectrally resolved, functional super-resolution microscopy reveals nanoscale compositional heterogeneity in live-cell membranes. *J. Am. Chem. Soc.* **2017**, *139*, 10944-10947.

(6) Xiang, L.; Chen, K.; Yan, R.; Li, W.; Xu, K. Single-molecule displacement mapping unveils nanoscale heterogeneities in intracellular diffusivity. *Nat. Methods* **2020**, *17*, 524-530.

(7) Cui, B.; Wu, C.; Chen, L.; Ramirez, A.; Bearer, E. L.; Li, W.-P.; Mobley, W. C.; Chu, S. One at a time, live tracking of NGF axonal transport using quantum dots. *Proc. Natl. Acad. Sci. U. S. A.* **2007**, *104*, 13666-13671.

(8) Tokunaga, M.; Imamoto, N.; Sakata-Sogawa, K. Highly inclined thin illumination enables clear single-molecule imaging in cells. *Nat. Methods* **2008**, *5*, 159-161.

(9) Zhang, Z.; Kenny, S. J.; Hauser, M.; Li, W.; Xu, K. Ultrahigh-throughput single-molecule spectroscopy and spectrally resolved super-resolution microscopy. *Nat. Methods* **2015**, *12*, 935-938.

(10) Choi, A. A.; Xiang, L.; Li, W.; Xu, K. Single-molecule displacement mapping indicates unhindered intracellular diffusion of small ($\lesssim$1 kDa) solutes. *J. Am. Chem. Soc.* **2023**, *145*, 8510-8516.

(11) Torra, J.; Viela, F.; Megias, D.; Sot, B.; Flors, C. Versatile Near-Infrared Super-Resolution Imaging of Amyloid Fibrils with the Fluorogenic Probe CRANAD-2. *Chem. Eur. J.* **2022**, *28*, e202200026.

(12) Rust, M. J.; Bates, M.; Zhuang, X. W. Sub-diffraction-limit imaging by stochastic optical reconstruction microscopy (STORM). *Nat. Methods* **2006**, *3*, 793-795.

(13) Huang, B.; Wang, W.; Bates, M.; Zhuang, X. Three-dimensional super-resolution imaging by stochastic optical reconstruction microscopy. *Science* **2008**, *319*, 810-813.

(14) Pei, S.-C.; Horng, J.-H. Circular arc detection based on Hough transform. *Pattern Recogn Lett* **1995**, *16*, 615-625.